Front. Earth Sci. 2021, 15(4): 817–830
https://doi.org/10.1007/s11707-021-0911-z

RESEARCH ARTICLE

Damage characterization of shale under uniaxial compression by acoustic emission monitoring

Huijun LU[1], Ru ZHANG (✉)[2], Li REN (✉)[2], Anlin ZHANG[1], Yiming YANG[1], Xiaopeng LI[2]

1 State Key Laboratory of Hydraulics and Mountain River Engineering, College of Water Resource & Hydropower, Sichuan University, Chengdu 610065, China
2 Key Laboratory of Deep Earth Science and Engineering (Ministry of Education), Sichuan University, Chengdu 610065, China

Abstract Understanding the damage behavior and cracking mechanism of brittle shale is crucial for hydraulic fracturing design. In this research, uniaxial compression tests are conducted on shale samples with different bedding plane orientations, and acoustic emission monitoring is implemented synchronously. The results indicate that the apparent elastic modulus increases with increasing bedding orientation. For the bedding orientations of 45° and 90°, the lateral deformation is anisotropic due to the bedding structure, revealing the anisotropic Poisson effect. A shear failure surface and tensile failure surfaces form parallel to the bedding plane for bedding orientations of 45° and 90°, respectively. For the bedding orientation of 0°, shear failure mainly occurs through the bedding planes. Additionally, the damage mechanism of shale is investigated by crack classification based on AE parameters. It is found that crack initiation is induced by the generation of shear cracks for the bedding orientation of 45°, whereas by the generation of tensile cracks for other bedding orientations. According to damage attributable to different type cracks, shear cracks dominate the damage behavior for bedding orientations of 0° and 45°, whereas tensile cracks dominate the damage behavior for bedding orientation of 90°. Finally, the information entropy is calculated by AE energy. A low value of information entropy, approximately 0.36, predicts failure with a low degree of instability for the bedding orientation of 0°, whereas a high value of information entropy, more than 1.5, predicts failure with a high degree of instability for other bedding orientations. This finding indicates that the failure behavior is gradual progressive damage for bedding orientation of 0°, whereas sudden damage dominates failure behavior for other bedding orientations.

Received January 9, 2021; accepted May 5, 2021

E-mails: zhangru@scu.edu.cn (Ru ZHANG)
renli-scu@hotmail.com (Li REN)

Keywords shale, damage characterization, uniaxial compression, acoustic emission

1 Introduction

In recent decades, the increasing fossil energy demand has driven the exploitation of unconventional hydrocarbon reservoirs, particularly oil and gas shale (Rybacki et al., 2016). Shale gas, a kind of clean energy, has attracted the attention of governments and scientists worldwide. With hydraulic fracturing technology, shale gas development has made significant progress in China. However, the hydraulic fracturing design is closely related to the mechanical properties of shale. Therefore, research on the mechanical properties and damage behavior of shale under the loading is crucial.

Shale is formed by the directional distribution of rock mineral particles, especially clay minerals, in the process of sedimentation (Johnston and Christensen, 1995; O'Brien and Slatt, 2012). Therefore, shale is generally regard layered shale as a transversely isotropic material to study its mechanical response after loading (Amadei, 1996; Hakala et al., 2007). Kim et al. (2012) investigated the anisotropic characteristics of the P-wave velocities, thermal conductivities and elastic moduli of the Boryeong shale occurring in South Korea. Triaxial compression tests under different confining pressures were performed by Niandou et al. (1997). The V-type of compressive strength and different failure modes were obtained and analyzed with the change in bedding orientation. Rybacki et al. (2015) conducted a series of mechanical tests on European black shales with varying mineralogy, water content, maturity and porosity properties, and studied the uniaxial and triaxial compressive strength, tensile strength and static Young's modulus at varying confining pressures, temperatures and strain rates. Heng et al. (2015) performed

direct shear tests on shale with different bedding plane orientations and obtained and analyzed the shear strength parameters and failure modes. Among the results, the shear strength was the lowest and the shear failure surface was the smoothest for the shale that underwent shear along the weak bedding. Hou et al. (2016) revealed the effect of the bedding orientation on the mechanical property and energy evolution characteristics of shales under uniaxial compression tests.

Despite the findings on the anisotropic mechanical properties revealed in the above researches, the analyses of the damage mechanism based on the failure mode and bedding structure were relatively weak. Acoustic emission (AE) monitoring and computed tomography (CT) scanning are the main methods used to capture the behavior of rock failure. Tensile failure and shear failure under high pressure waterjet impinging were revealed by CT scanning (Sheng et al., 2017). Wu et al. (2017) performed uniaxial compression experiments to study the characteristics of AE data collected during the failure process of shale rocks. The testing results indicated that the AE rates and energy values increased markedly when slippage occurred and that these parameters reflected the generation of microcracks in the rock. In addition, Li et al. (2017) revealed the change law of AE events as an indicator of the closure of pores with high aspect ratios and the evolution of the microstructure induced under an elevated stress field in Sinian shale. The failure mechanism of anisotropic shale during Brazilian testing was analyzed based on AE information (Simpson et al., 2014; Wang et al., 2016; Yang et al., 2019). Simultaneous recording of AE showed that the AE activity coincided with the fracture evolution process and changed with bedding orientation. Overall, the above studies confirmed that AE parameter can effectively reflect the generation of microcracks.

However, fractures in shale gas reservoirs are often formed by not only tensile failure but also shear failure. Nevertheless, the effect of bedding structure on the generation of different crack types (mode-I opening tensile cracks and mode-II shear cracks) under a certain stress field has rarely been researched and considered in studies on shale. Furthermore, the dominance of damage corresponding to these typical crack types urgently need to be determined under different loading stages. On the other hand, the artificial fracturing of shale reservoirs causes local stress concentrations in the shale, which ultimately causes failure. The difference in the effect of bedding structure is necessary to consider to accurately predict rock failure and evaluate failure behavior of shale. Therefore, considering the bedding effect in the study of damage behavior and mechanism will improve engineering practice. In terms of the crack types formed in the process of concrete fracture, a method for crack classification based on AE parameters was suggested by JCMS-Ⅲ B5706 (2003). Afterwards, the code has been widely used and optimized by many scholars (Ohno and Ohtsu, 2010; Hu et al., 2019; Jia et al., 2020). Regarding rock failure, Sethna et al. (2001) indicated that a small disturbance during the critical state can cause a series of sudden avalanche instabilities, resulting in avalanche events across multiple orders of magnitude. Thus, the continuous application of a load will lead to the sudden failure of a rock material. The physical response during avalanche events was characterized using the AE energy, counts and amplitude (Nataf et al., 2014). Therefore, the evolution process from a stability state to an instability state with information transmission can be researched by information entropy (Shannon, 1948), which can quantitatively describe the failure process.

Therefore, in this paper, cubic shale samples with three typical bedding plane orientations (0°, 45°, and 90°) were prepared, and laboratory tests were conducted under uniaxial compression. During the tests, the DH3818Y static strain system and AE system were used to record the deformation and AE information during the damage process, respectively. Combining the measured anisotropic mechanical parameters and observed failure modes, the different cracks were classified to emphatically analyze the damage behavior and cracking mechanism under the effect of bedding structure based on AE information. Additionally, predicting rock failure and evaluating failure behavior of shale were studied through information entropy.

2 Material and methods

2.1 Samples

The damage behavior and cracking mechanism of shale under the uniaxial compression were investigated. The shale blocks with obvious sedimentary bedding planes were obtained from Chongqing, southwest China. The main constituents of the obtained shale are quartz (approximately 72.4%), clay (approximately 11.7%) and carbonates (approximately 13%). According to the following formula:

$$BI = \frac{W_{\text{quartz}}}{W_{\text{quartz}} + W_{\text{carbonate}} + W_{\text{clay}}}, \quad (1)$$

where BI is brittleness index and W_{quartz}, $W_{\text{carbonate}}$, and W_{clay} are the contents of quartz, carbonate, and clay, respectively.

The brittleness index of the shale is calculated to be 74.56%, reflecting the high brittleness index of the shale samples (Jarvie et al., 2007). To accurately measure the anisotropic deformation by using stain gauge as shown in Fig. 1(a), cubic samples of approximately 50 mm long, 50 mm wide, and 100 mm high with different bedding plane orientations (0°, 45°, and 90°) were cut from same block and shown in Fig. 1(b). The bedding plane orientation is the angle between the bedding plane and the horizontal plane.

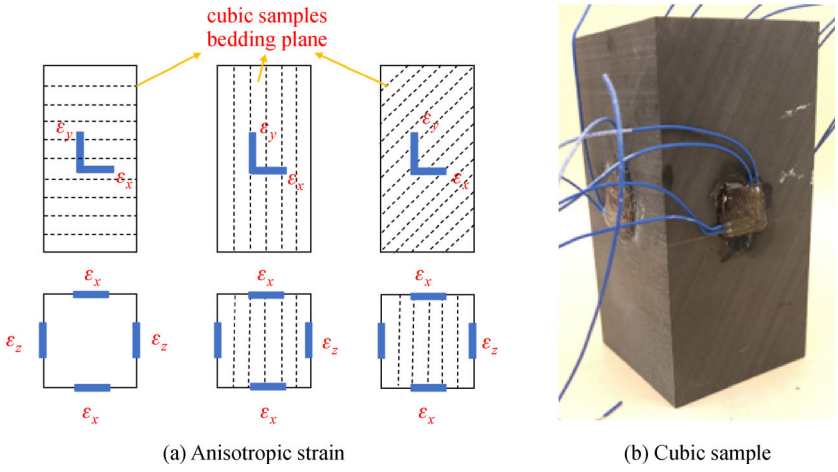

Fig. 1 The diagrams of anisotropic strain and cubic shale sample.

2.2 Experimental procedure

The experimental system (Fig. 2) was used to investigate deformation and failure behavior during the uniaxial compression on shale samples. The loading was applied using the MTS 815 rock mechanics test system in the Key Laboratory of Deep Earth Science and Engineering, Sichuan University. The lateral and axial strain gauges were pasted on the four side centers of sample and coated with silica gel to protect them. Then the strain data are recorded using a DH3818Y static strain system. And eight acoustic emission sensors of PAC AE system were asymmetrically mounted on the end of sample to detect and record the AE signals. Each signal was amplified by a preamplifier with an amplification of 40 dB. The test was then continued and loaded until failure with a loading rate of 0.04 mm/min in the axial direction.

2.3 Anisotropy in shale elasticity, strength and failure pattern

Shale is regarded as a transversely isotropic material. The anisotropic deformation of shale is described in a Cartesian coordinate system as shown in Fig. 3. θ is the angle between the bedding plane and the horizontal plane. The y direction is consistent with the axial load direction, the z direction is always parallel to the bedding planes, and the x direction is at an angle of θ to the bedding plane.

Figure 4 shows the stress-strain curves of the shale samples with the three bedding orientations under uniaxial compression. There is basically no initial compaction stage, indicating that the shale samples are dense. The shale samples are destroyed at the peak strength without a post-peak stage, reflecting a brittle failure manner. The apparent elastic parameters are extracted by the linear

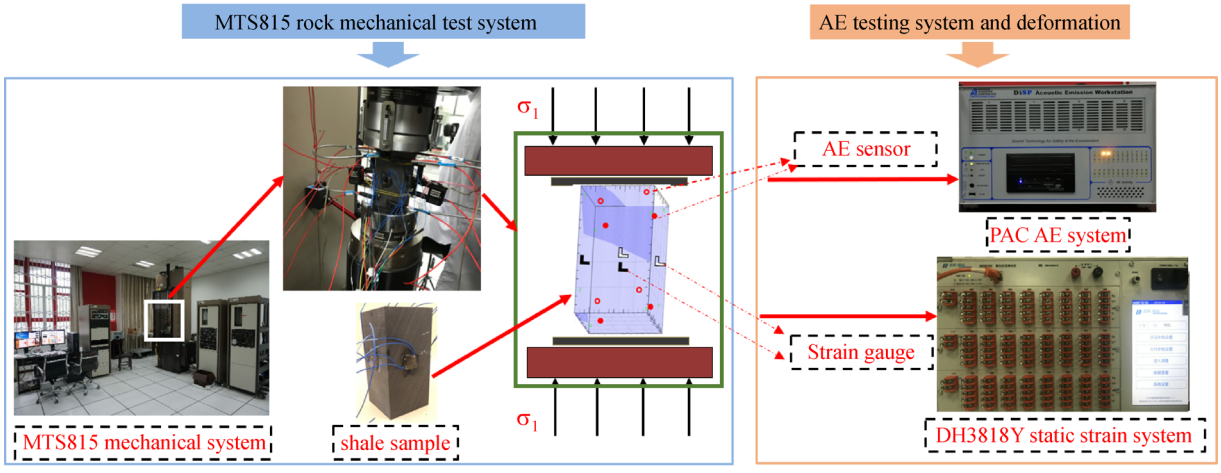

Fig. 2 Experimental system for this paper.

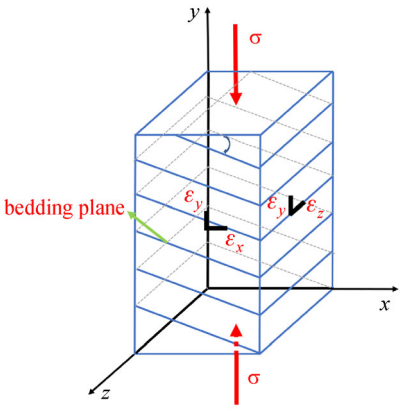

Fig. 3 Loading diagram of transversely isotropic shale in the Cartesian coordinate system.

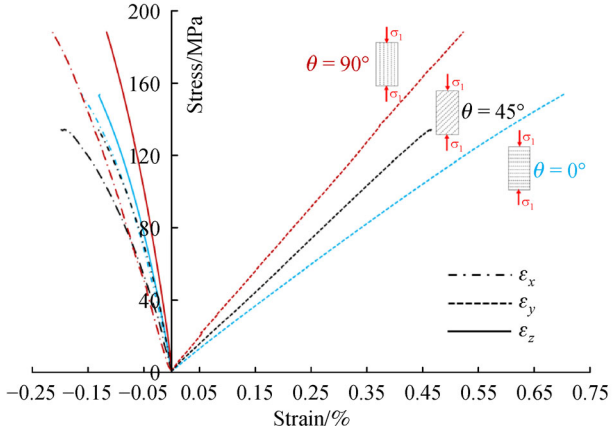

Fig. 4 Stress-strain curves of the shale samples with different bedding orientations (the blue line, black line, and red line represent the data of 0°, 45°, and 90° orientations, respectively).

elastic stage of stress and strain, as shown in Table 1. Clearly, the apparent elastic modulus, E_y, increases with the increasing bedding orientation. The E_y of 90° bedding orientation is 1.56 times larger than that of 0° bedding orientation. During the initial stage of loading, ε_x and ε_z are basically consistent for the bedding orientation of 0°. Nevertheless, they are very different for other bedding orientations, resulting in an anisotropic apparent Poisson's ratio. v_{xy} is always larger than v_{zy} for bedding orientations of 45° and 90°. The ratio of v_{xy} and v_{zy} is 1.52 for the bedding orientation of 90°, which is the largest ratio.

As a whole, the bedding orientations of 90° and 0° correspond to the maximum and minimum elastic modulus, respectively. Therefore, the degree of anisotropy is calculated to be 1.64 with the following expression (Worotnicki, 1993):

$$R_t = \frac{E_{c\max}}{E_{c\min}}, \tag{2}$$

where R_t is the degree of anisotropy and $E_{c\max}$ and $E_{c\min}$ are the maximum and minimum elastic modulus of the shale samples, respectively.

According to the classification of anisotropy in Worotnicki (1993), the degree of anisotropy of the shale samples is moderate in this paper.

Regarding the uniaxial compressive strength of the shale samples, as shown in Fig. 5, among the different bedding orientations tested, the bedding orientations of 90° and 45° correspond to the maximum and minimum uniaxial compressive strengths, respectively. As a whole, the variation in compressive strength exhibits a V-type pattern with different bedding orientations and is consistent with the result of Hou et al. (2016).

The typical failure modes of shale with different bedding orientations under uniaxial loading are divided into three types, as shown in Fig. 6. For the bedding orientation of 0°, the shear and tensile failure modes show that multiple failure planes pass through the bedding planes, resulting in numerous broken blocks, whereas the main shear failure mode for the bedding orientation of 45° is expressed at the end of the sample due to bedding shear slip, and that several fractures pass through the bedding planes. Clearly, for the bedding orientation of 90°, the tensile failure shows that the fracture is formed along the bedding plane. As the load increases, the development of lateral expansion increases the transverse tensile stress, resulting in macrocracks propagating along the weak bedding planes. Therefore, the shale matrix separates into independent bands, and buckling failure occurs under compression. Due to the deformation resistance of the shale matrix that

Table 1 The shear strength parameters of the shale samples

Sample number	θ/(°)	E_y/GPa	v_{xy}	v_{zy}	v_{xy}/v_{zy}
0-1	0	23.75	0.12	0.12	1.00
0-2	0	23.32	0.17	0.16	1.06
45-1	45	29.09	0.24	0.17	1.41
45-2	45	29.29	0.18	0.15	1.20
90-1	90	35.74	0.35	0.20	1.75
90-2	90	36.25	0.25	0.17	1.47
90-3	90	38.15	0.27	0.20	1.35

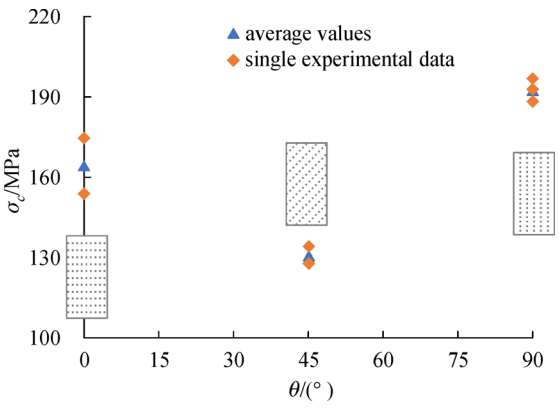

Fig. 5 Uniaxial compressive strength of shale samples with different bedding orientations.

must be overcome to failure, the shale samples with the bedding orientation of 90° possesses the maximum compressive strength and elastic modulus.

3 Damage behavior using AE monitoring

3.1 AE parameters characteristics

According to real-time AE information, the AE counts and energy are calculated to describe the internal activity of shale during the process of uniaxial compression. The AE parameters, AE counts and energy, are shown in Fig. 7. Clearly, due to few of the original microcracks and micropores in the shale close during the initial stage of uniaxial loading, the cumulative AE counts and energy are relatively small and increase slowly. Subsequently, the cumulative AE counts and energy curves are nearly horizontal because the deformation of shale samples enters the linear elastic stage, reflecting the generation of very few microcracks in the shale. During crack initiation, the variations in cumulative AE counts and energy increase and become stepwise for bedding orientations of 45° and 90°, while the increasing regularity corresponding to the bedding orientation of 0° is continuous. Finally, quick

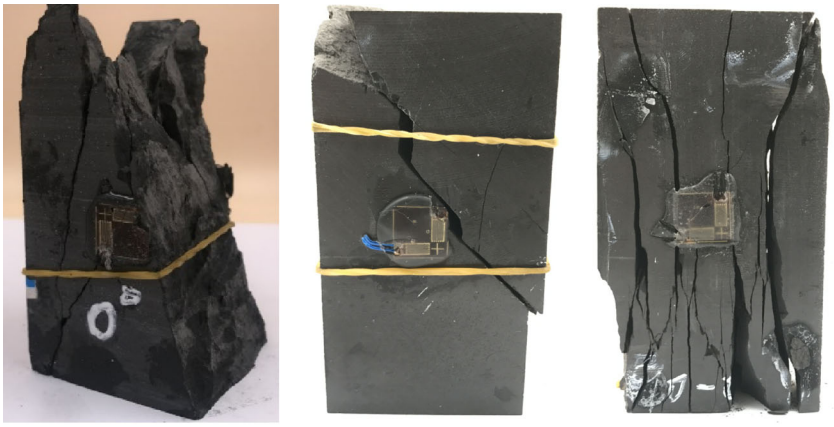

(a) 0° (b) 45° (c) 90°

Fig. 6 Failure patterns of the shale samples with different bedding orientations.

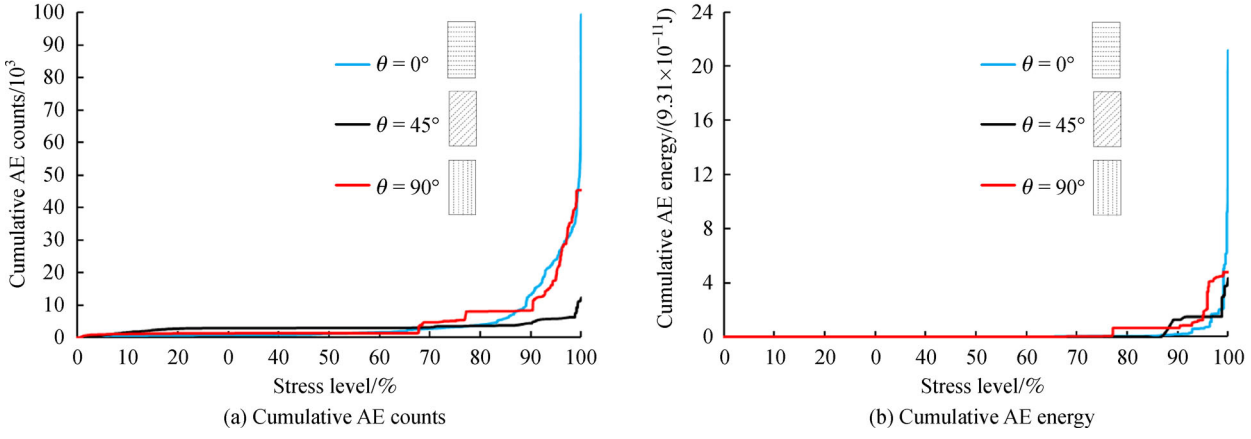

(a) Cumulative AE counts (b) Cumulative AE energy

Fig. 7 AE parameters for the three bedding orientations under uniaxial loading.

increases in AE counts and AE energy are measured with the generation of macrocracks before the peak compressive strength. However, the cumulative values change in AE counts and energy corresponding to the bedding orientation of 0° are considerably larger than those of other bedding orientations near the peak strength. This difference in AE energy is approximately one order of magnitude and is related to failure degree of the shale.

3.2 Spatial evolution of different types of cracks

To date, most studies on the anisotropic failure behavior of shale have focused on the phenomenological description of the destruction pattern or the analysis of anisotropic mechanical parameters, without a deep analysis of the micro-mechanism. Therefore, the evolution of tensile and shear cracks in shale is studied to analyze the failure micro-mechanism under uniaxial loading based on AE information.

Ohtsu et al. (1998) used the crack classification method presented in (JCMS-III B5706, 2003) to well analyze the failure mechanism of concrete in uniaxial compression test, and the results were confirmed under the four-point bending tests and the direct shear tests of concrete specimens. To classify active cracks, AE parameters shown in Fig. 8 of the rise time and the amplitude are applied to calculate RA value, and the average frequency is obtained from AE counts and the duration time as follow functions 3 and 4. In Fig. 8, AE count is the number of oscillations of the signal crossing the threshold. AE amplitude is maximum amplitude of AE event signal waveform. Rise time is the time interval between the first time the event signal crosses the threshold and the maximum amplitude history. Duration time is the time interval between the event signal first crossing the threshold and finally falling the threshold:

$$\mathrm{RA} = \text{rise time}/\text{amplitude}, \tag{3}$$

$$\mathrm{AF} = \text{AE counts}/\text{duration time}. \tag{4}$$

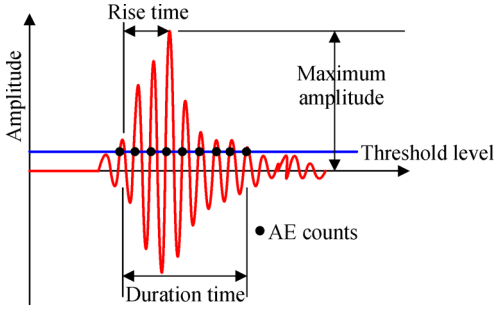

Fig. 8 AE parameters in an AE hit (Ohno and Ohtsu, 2010).

The tensile cracks in concrete material mostly correspond to high AF values and low RA values, whereas shear cracks possess high RA values and low AF values, which are similar to the trends observed in rocks (Ohno and Ohtsu, 2010; Du et al., 2020). Therefore, cracks in concrete can be classified into tensile and shear cracks with RA and AF parameters, as illustrated in Fig. 9(a). However, Du et al. (2020) conducted a series of rock tests, including Brazilian indirect tension test, three-point bending test, modified shear test and uniaxial compression test to investigate crack classification. It is indicated that when the AF values are smaller than K1, the type crack is shear crack. And the value of K1 is less than 100 kHz. Therefore, Du et al. (2020) modified the distribution mode of AF-RA data shown in Fig. 9(b) to distinguish the shear and tensile cracks.

The distribution characteristics of AF and RA for different orientations of shale samples are shown in Fig. 10. Clearly, the AF values are distributed mostly in the range of 100–160 kHz, and its largest proportion is mainly concentrated in the range of 120–140 kHz for all bedding orientations tested. For the bedding orientation of 90°, the proportion of AE events is 33.55% in the interval of 120–140 kHz, which is considerably larger than that of other bedding orientations and other AF intervals. For the AF interval below 40 kHz, the proportion of AE events is low, especially for bedding orientations of 45° and 90°.

As indicated in Fig. 10(b), the RA is generally concentrated below 7 ms/V for the bedding orientation of 90°. And the proportion of AE events in the interval of 1–3 ms/V, more than 46%, is far larger than those in other intervals. For the bedding orientations of 0° and 45°, the

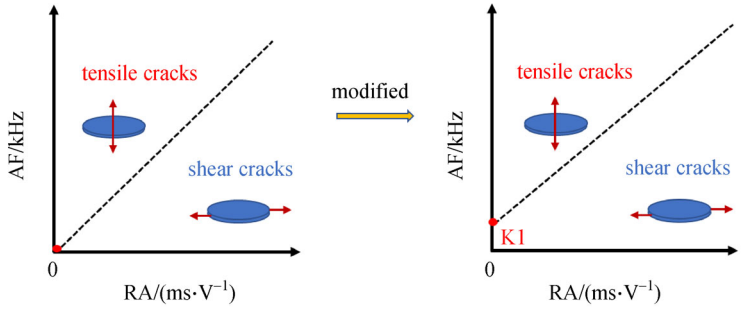

Fig. 9 Crack classification based on AF–RA correlation analysis for different materials.

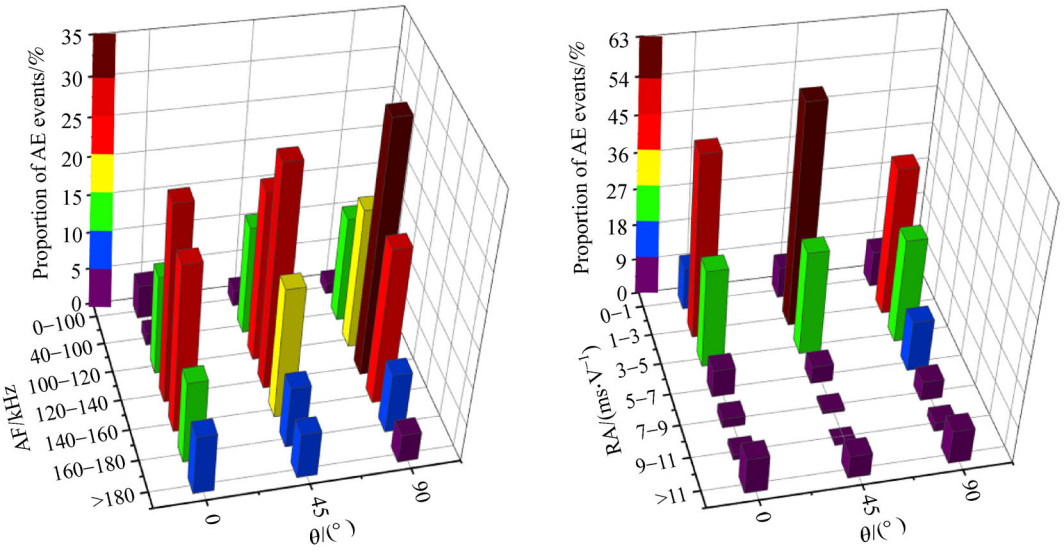

(a) The distribution of AF (b) The distribution of RA

Fig. 10 The distributions of AF and RA for different orientations of shale samples.

proportion of AE events in the range of 1–3 ms/V is largest.

Overall, the distribution characteristics of *AF* and *RA* can be determined by the propagation speed and the scale of cracks (including the number of cracks). The high extension speed and low extension scale of cracks will induce AE signals with high *AF*. Furthermore, tensile cracking usually has a higher extension speed and lower extension scale than shear cracking. Therefore, higher *AF* events are tensile cracks (Du et al., 2020). According to the main tensile failure mode for shale samples with 90° bedding orientation, the proportion of AE events is 1.42% when the *AF* value is lower than 40 kHz, whereas the proportion of AE events is 13.99% when the *AF* value is in the interval of 40–100 kHz. Therefore, the *AF* value of point K1 can be confirmed as 40 kHz, reflecting few shear cracks. On the other hand, the most important distribution interval of *AF* and *RA* is used as the dividing line. The proportion of *AF* and *RA* are concentrated in the interval of 120–140 kHz and below 7 ms/V for the bedding orientation of 90°, respectively. In this case, the boundary between shear cracks and tensile cracks is determined be

$$AF = \frac{130}{7}RA + 40. \tag{5}$$

To maintain the consistency of the method, the proportion of *AF* is also concentrated in the interval of 120–140 kHz and the *RA* is basically distributed in the interval of 1–3 ms/V for the bedding orientations of 0° and 45°, thus, in this case, the boundary between shear cracks and tensile cracks is determined as

$$AF = \frac{130}{3}RA + 40. \tag{6}$$

Hence, statistical analyses of AE events are conducted for crack classification of the shale samples with different bedding orientations, as shown Fig. 11. It shows that the

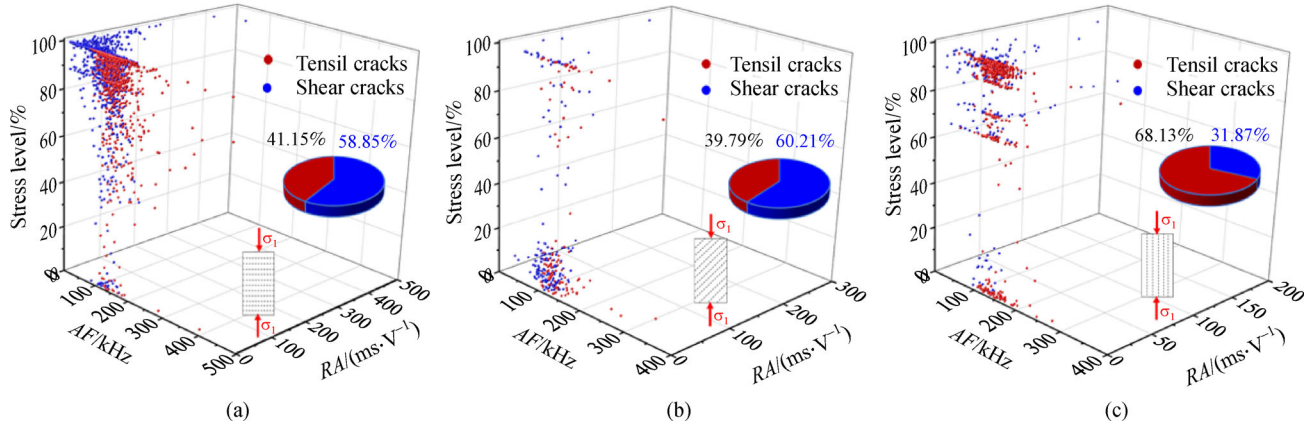

(a) (b) (c)

Fig. 11 Crack classification for different bedding orientations under the process of loading.

proportion of AE events for tensile cracks is 68.13% for the bedding orientation of 90°, whereas that for shear cracks is 58.85% and 60.21% for bedding orientations of 0° and 45°, respectively. The statistical results are consistent with the main failure mode. Hence, the reliability and accuracy of the above dividing lines are further confirmed. The number of AE events can describe the frequency of internal activity, reflecting that the activity frequencies corresponding to bedding orientations of 0° and 90° are higher than that corresponding to bedding orientation of 45°. Similarly, few AE events occur during the linear elastic deformation stage for all bedding orientations. The AE events basically concentrated in the late loading stage for bedding orientations of 0° and 90°. By contrast, a majority of AE events appear in the early loading stage for the bedding orientation of 45°. Therefore, the number of AE events cannot reflect the degree of damage.

Compared with AE counts, AE energy has smaller dependence on the voltage threshold and working frequency during the test period. Therefore, AE energy can better reflect the processes of rock deformation, damage and failure. It has been widely used to quantitatively evaluate the rock damage (Tian et al., 2020). To further investigate the micro-mechanism of failure, the spatial evolution of AE events and their corresponding energy characteristics are analyzed, as shown in Fig. 12. The letters S and T represent tensile cracks and shear cracks, respectively. A larger sphere with a darker color indicates that the AE energy of AE event is greater. To optimize the analysis, the different loading intervals of normalized peak stress are selected as 0–30%, 30%–70%, 70%–90%, 90%–95% and > 95% of the peak strength (to failure).

Figure 12 clearly shows that different microcracks are randomly distributed in the shale samples and the AE energy of AE events is very low before 70% of the peak strength. From 95% of the peak stress to the failure stage, the AE energy is high and relatively concentrated, while the distributed pattern of high AE energy is basically consistent with the main tensile and shear failure patterns for different cracks. Hence, the classification of shear and tensile crack is accurate by AE parameters. On the other hand, the distribution characterize of AE energy can be summarized from the disordered state of low AE energy to an ordered state with high AE energy until the failure. And the high AE energy can predict the generation of macroscopic fracture.

3.3 Damage behavior based on AE energy

When the cross-sectional area of the intact material completely loses its bearing capacity, the cumulative AE energy is E_c. If the cross-sectional area is damaged at any time, the corresponding AE energy is E_d. Hence, at any

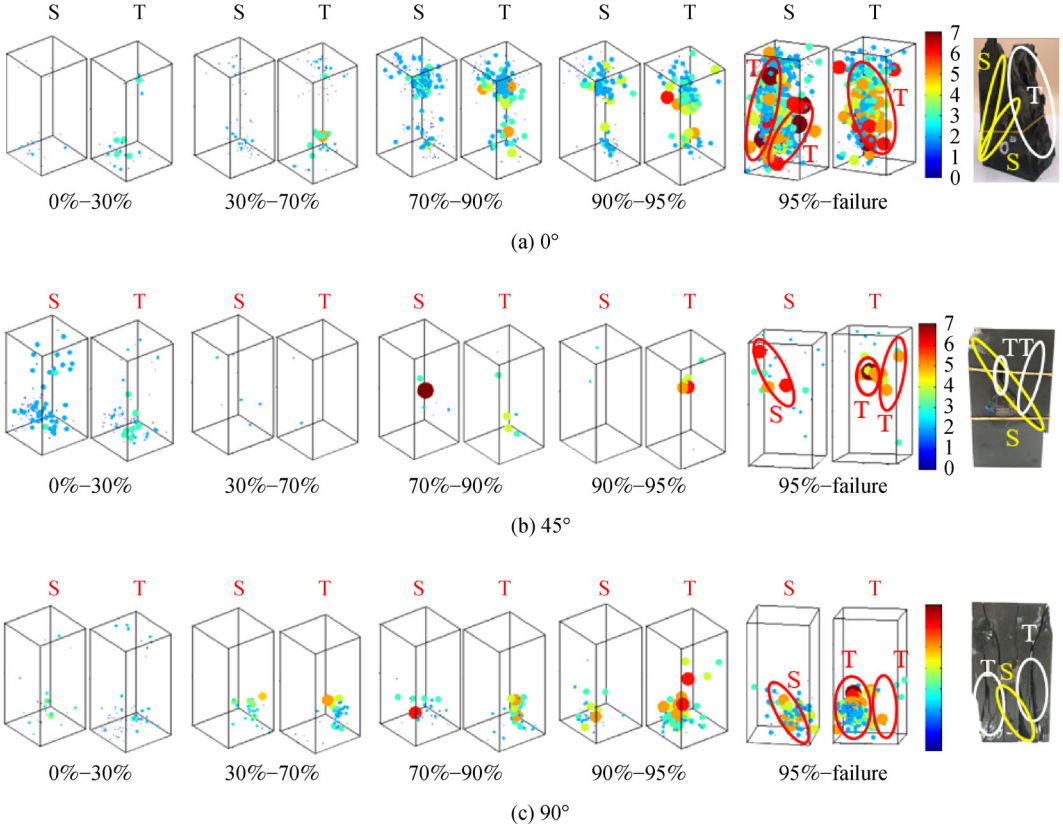

Fig. 12 The spatial evolution of AE energy for different cracks under different loading intervals.

time, the shale damage variable, D, can be calculated based on AE energy as following formula (Tian et al., 2020):

$$D = \frac{E_d}{E_c}. \tag{7}$$

From the mesoscale perspective, the failure of microcracks in rock is a mixed mode fracture (mode I opening tensile cracks and mode II shear cracks) problem (Yuan et al., 2012). In Fig. 12, each AE event is classified as a shear crack or tensile crack. Figure 12 indicated that each AE event has different characteristics of AE energy. Therefore, the different degrees of shear and tensile cracking have different AE energy characteristics. In other words, the contribution of tensile and shear cracks to shale damage can be calculated by considering the AE energy:

$$D_{\mathrm{T}} = \frac{E_{\mathrm{T}d}}{E_c},\ D_{\mathrm{S}} = \frac{E_{\mathrm{S}d}}{E_c}, \tag{8}$$

where D_{T} and D_{S} are the contribution degrees of damage for tensile and shear cracks, respectively. $E_{\mathrm{T}d}$ and $E_{\mathrm{S}d}$ are the cumulative tensile AE energy and cumulative shear AE energy of the shale sample before a certain time, respectively.

The damage evolution curves are obtained according to the above calculation method, as shown in Fig. 13. To better observe and analyze the damage behavior, the late loading stage is enlarged. The existence of original microcracks in the shale can be regarded as initial damage. The AE events of low AE energy are caused by the closure of the few original microcracks, resulting in minor damage. During the process of linear elastic deformation, the amount of damage induced is extremely small. As the crack initiation stress is approached, the stored elastic energy is released, resulting in a high AE energy. Nevertheless, the type of cracks inducing crack initiation are different under the effect of bedding structure. After crack initiation, the shale samples adjust to maintain stability, resulting in a constant amount of damage. This stage is called the quiet period of AE activity. Just before failure, the damage increases quickly with the macroscopic propagation of both tensile and shear cracks.

As the AE energy increases considerably after crack initiation, crack initiation can be identified by the sudden increase in AE energy (Tian et al., 2020). Figure 14(a) shows that the stress level of corresponding to crack initiation decreases with increasing bedding orientation. However, the crack initiation stress curve is V-shaped, similar to the trend of compressive strength, indicating that

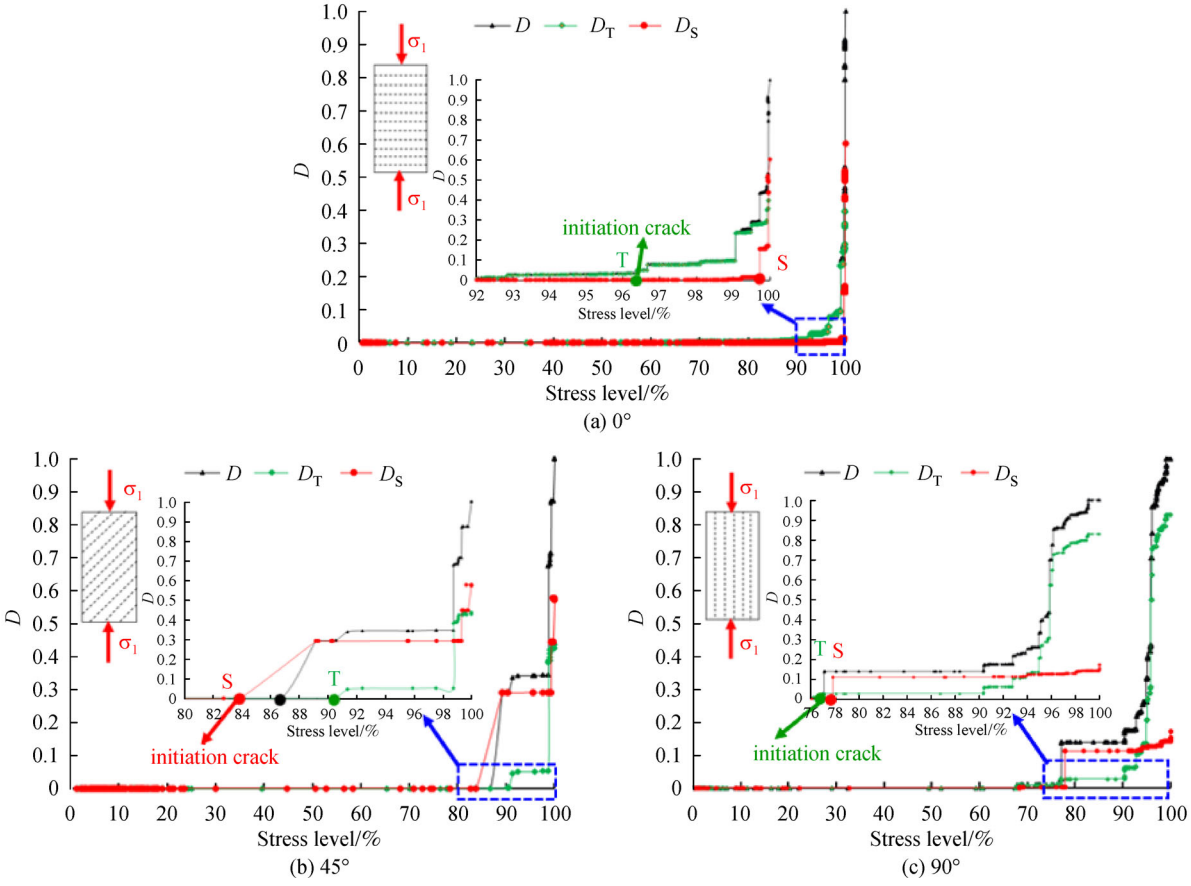

Fig. 13 Damage evolution of shale with different bedding orientations during the loading process.

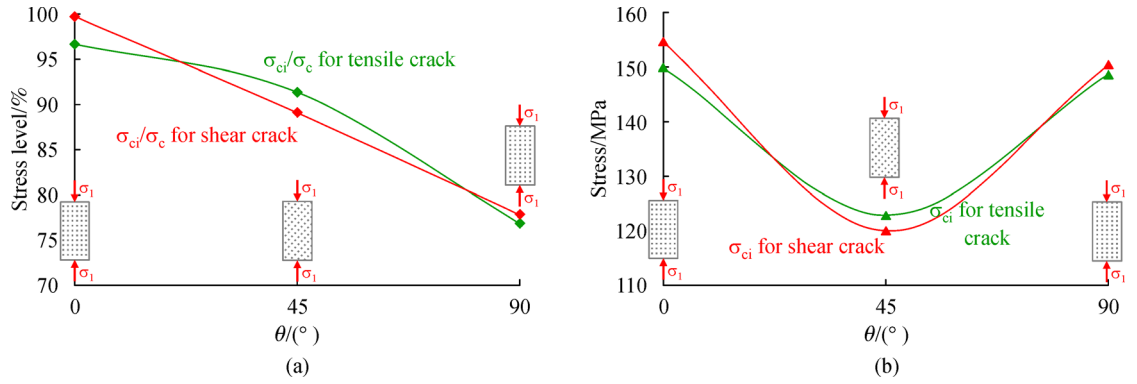

Fig. 14 The stress level and crack initiation stress for different types of microcracks. (a) The stress level corresponding to crack initiation; (b) The crack initiation stress.

the bedding orientation of 45° more easily cracks. In addition, for the bedding orientation of 45°, the initiation of cracks is prioritized by shear cracks, while the other bedding orientations exhibit the initiation of predominantly tensile cracks.

Figure 15 shows the proportion of damage corresponding to different types of cracks before the peak stress. Clearly, shear cracks dominate the damage behavior for bedding orientations of 0° and 45°. However, the proportion of tensile damage is 82.80% for bedding orientation of 90°. Therefore, the type of crack that statistically dominates the damage is consistent with the main failure pattern observed.

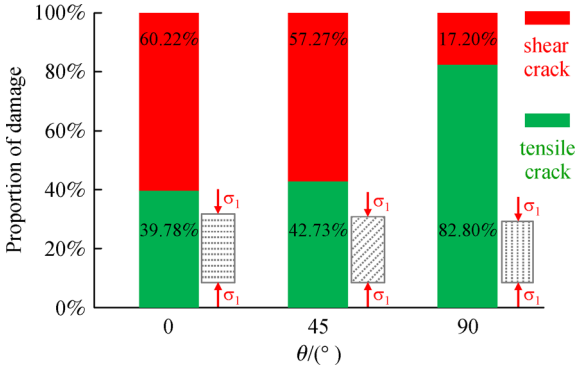

Fig. 15 The proportion of damage before the peak stress for different types of microcracks.

According to the analysis of the failure behavior of anisotropic shale in Jaeger (1960), the difference in crack initiation and damage for different microcracks under the effect of bedding structure is further explained.

Under uniaxial compression, when the angle between the bedding plane and principal stress satisfies certain conditions, the normal and tangential stresses acting on the layer reach the yield condition, resulting in plastic slipping along the bedding plane (Zhu and Zeng, 2005). In this paper, the shale with bedding orientation of 45° exhibits above phenomenon. This reasonably indicates that shear cracks are the first to initiate and dominate damage behavior. Therefore, the bedding plane and potential failure surface are coincident for the bedding orientation of 45°. Meanwhile, the potential shear failure surface through the shale matrix for the bedding orientation of 0° requires a large shear stress component. However, the lateral expansion under axial loading results in tensile damage, and tensile cracks initiate first. As the uniaxial stress increases, the shear cracking increases in scale, and shear cracks dominate the failure behavior near the peak strength.

However, for the bedding orientation of 90°, the weak bedding planes compete with the potential shear failure surface under the condition of lateral expansion due to axial loading. Due to the low amount of cementation between the weak bedding plane and shale matrix, tensile damage occurs more easily perpendicular to weak bedding plane, resulting in bands of shale matrix with high compressive strength forming in the shale. Therefore, tensile failure perpendicular to weak bedding plane is the main failure mode. Before failure, the tensile damage and shear damage increase with the instability of these shale matrix bands and progressive damage of the weak bedding planes. However, in general, tensile cracks are first to initiate and dominate the damage behavior.

4 Predicting rock failure and exploring failure behavior of the shale based on information entropy

According to above study, the failure process in shale samples is from microcrack generation in a disordered state to the macrocrack generation in an ordered state. To investigate precursor of rock failure and failure behavior of shale under the effect of bedding structure, the information entropy is used to reveal the evolution characteristics of shale failure based on AE energy.

4.1 Calculation of information entropy based on AE energy

Information entropy, a measure of the certainty of state information, was proposed by Shannon (1948). The distribution characteristics of AE energy can be summarized as reflecting the damage process from a disordered state of low AE energy to an ordered state of high AE energy until failure of shale. In other words, the evolution of AE energy can describe the information from the stability state to the instability state. Hence, the information entropy can be used to describe the rock failure process in this paper. According to the concept of information entropy, the AE energy cluster can be regarded as a discrete sample space E_N, and the possible value of E belongs to $\{E_1, E_2, E_3, ..., E_n\}$ ($n \in N$). And the E_n is the AE energy of the nth AE event. N represents the number of AE events. The probability, P_i, should satisfy the following condition:

$$0 < P_i < 1(i = 1,2,3,...,n),\ \sum_{i=1}^{n} P_i = 1. \tag{9}$$

Meanwhile, P_i can be described as the proportion of AE energy of any independent interval in the AE energy cluster which is written as

$$P_i = \frac{E_{tc}}{E_c} \times 100\%, \tag{10}$$

where E_{tc} is the cumulative AE energies before a certain time.

Therefore, the uncertainty in each AE energy value in an independent interval depends on the probability P_i of the corresponding value. The average information of all the results E_i in test sample space E can be expressed by information entropy:

$$H(A) = -\sum_{i=1}^{n} P(E_i)\log_{10}P(E_i). \tag{11}$$

Notably, the generation of cracks is accompanied by the dissipation of energy, resulting in AE signal. More dissipate energy, resulting in a larger AE energy. Therefore, the state of the dissipative structure from stability to instability can be described by information entropy based on AE energy. Moreover, a low value of information entropy represents a stability state, whereas a high value represents an instability state.

4.2 Precursor and behavior of shale failure

The evolution process of a complex dynamic system can be directly reflected by the change in information entropy based on AE energy. A sliding window of a constant time series is set to calculate the information entropy, as shown in Fig. 16. This indicates that the low value of information entropy reflects the disordered state, corresponding to the slow generation of internal defects before crack initiation. The structure of shale is stable and stores elastic strain energy. Then, the information entropy suddenly increases at the critical point of crack initiation, reflecting the instability state of the dissipative structure. The information entropy begins to change in a zigzagging pattern, and the maximum value of each zigzag is basically the same except for those of the shale sample with bedding orientation of 0°, which slowly increases. Afterward, the information entropy increases again with the generation of macrocracks. Finally, the substantial increase of information entropy reveals a large number of macrocracks generated, resulting in instability destruction of the dissipative structure at the peak strength. To further analyze the difference in the critical point (the points of crack initiation, macrocrack generation and peak strength) under the effect of bedding structure, the stage of late loading is lengthened, as shown in Fig. 16, and the corresponding critical eigenvalues are given in Table 2.

Combining results shown in Fig. 16 and Table 2, for the critical point of crack initiation, the stress level decreases with increasing bedding orientation, which is consistent with Fig. 14(a). The information entropy and the degree of instability for bedding orientations of 45° and 90° is larger than that of bedding orientation of 0°. Furthermore, the critical point of macrocrack generation close to the peak strength can be regarded as the prediction point of shale failure, and the information entropy increases with increasing bedding orientation. For bedding orientation of 0°, the value of information entropy, approximately 0.36, is minimal and predicts failure with a minimum degree of instability. However, the phenomenon of the maximum cumulative AE energy corresponding to the minimum information entropy further reveals that the failure behavior is sudden through shale matrix. For other bedding orientations, a higher information entropy, more than 1.5, predicts failure with a high degree of instability, reflecting gradual progressive failure. At the critical point of peak strength, the information entropy is maximized and increases with the increasing bedding orientation. In terms of the failure mode, the shale with bedding orientation of 45° exhibits a single shear failure surface, whereas four main tensile failure surfaces are observed for the bedding orientation of 90°. Moreover, the more macro-failure surfaces there are, the higher the degree of instability of the dissipative structure.

5 Conclusions

In this paper, the anisotropic characteristics of shale samples were experimentally investigated in terms of their mechanical parameters and failure modes under uniaxial compression. Based on the AE information, the damage behavior and cracking mechanism were further analyzed. The main results of this study are summarized as

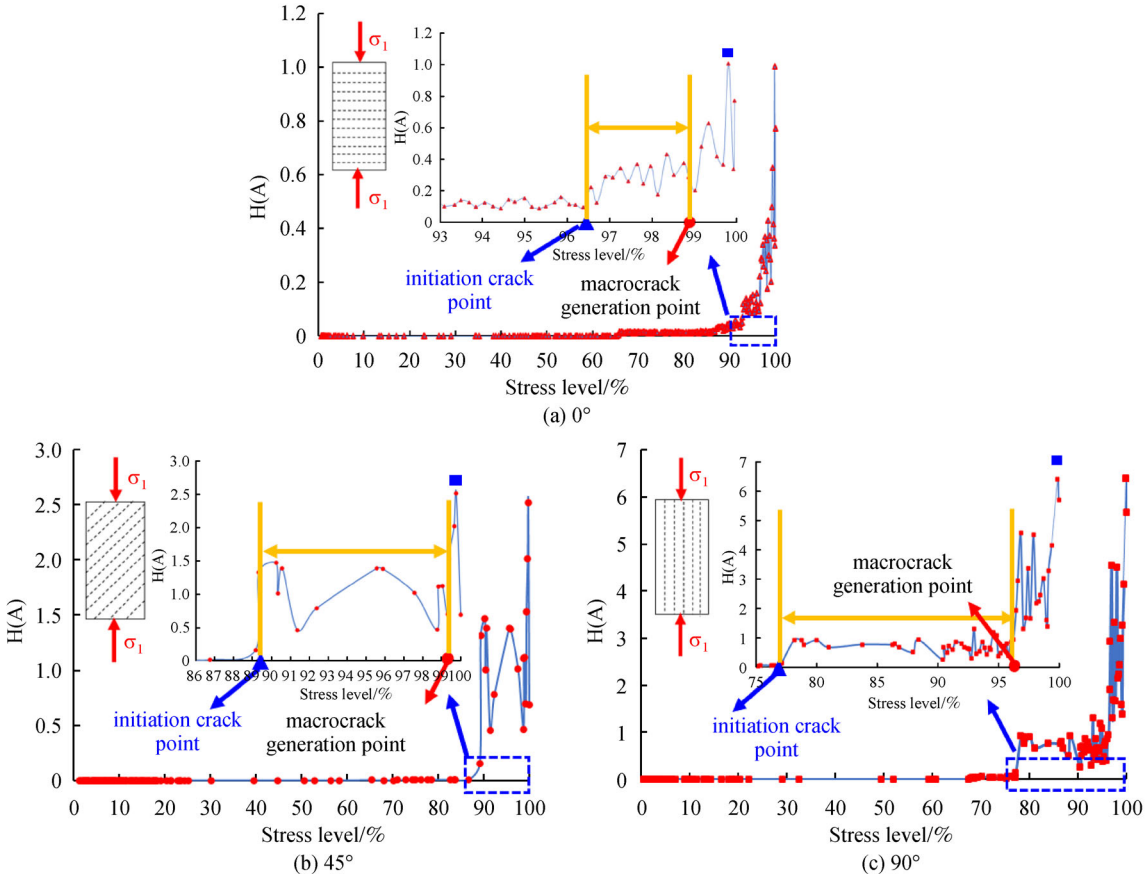

Fig. 16 The variations in entropy under different stress levels for the shale samples with different bedding orientations. (a) 0°; (b) 45°; (c) 90°.

Table 2 Stress level and information entropy for different critical points

θ/(°)	Crack initiation Point		Macrocrack generation point		Peak information entropy at peak strength point
	Stress level/%	Information entropy	Stress level/%	Information entropy	
0°	96.38	0.12	98.75	0.36	1.00
45°	89.32	1.31	99.38	1.53	2.51
90°	78.16	0.92	96.85	4.50	6.39

follows.

The variation in compressive strength with increasing bedding orientation is V-shaped, and the ratio of the maximum and minimum strength is 1.67. The apparent elastic modulus, E_y, increases with increasing bedding orientation. For the bedding orientations of 45° and 90°, the lateral deformation is anisotropic under the effect of bedding structure, revealing the anisotropic Poisson effect. Regarding the main failure mode, the shear failure surface and splitting tensile failure surface were parallel to bedding plane for bedding orientations of 45° and 90°, respectively. The shear failure for the bedding orientation of 0° mainly through the shale matrix.

To reveal the microscopic mechanism of the above anisotropic failure modes and damage behavior, AE information was analyzed to reflect the internal damage of shale. The statistical analyses of AE events were conducted based on the diving line between RA and FA for crack classification. The distribution pattern of high AE energy events for tensile cracks and shear cracks agrees with the tensile failure mode and shear failure mode, respectively. According to damage attributable to different types of cracks, shear cracks dominated the damage behavior for bedding plane orientations of 0° and 45°, whereas tensile cracks dominated the damage behavior for the bedding orientation of 90°. In addition, the inducing factor of crack initiation was the generation of shear cracks with high AE energy for the bedding orientation of 45° and the generation of tensile cracks with high AE energy for other bedding orientations, respectively. Meanwhile, the

Jager failure criterion was used to analyze the mechanism of crack initiation under the effect of bedding structure and further confirms the above research results.

The information entropy was calculated to predict rock failure and explore failure behavior of shale under the effect of bedding structure based on AE energy. The results show that a low value of information entropy, approximately 0.36, predicted failure with a low degree of instability for the bedding orientation of 0°, whereas a high value of information entropy, more than 1.5, predicted failure with a high degree of instability for other bedding orientations. Additionally, the failure behavior was gradual progressive damage for bedding orientation of 0°, whereas sudden damage dominated the failure behavior for other bedding orientations.

Acknowledgements The authors express their sincere gratitude to all the anonymous reviewers for their comments devoted to improving the quality of the paper. This work was supported by the National Natural Science Foundation of China (Grant No. 51704198) and the Department of Science and Technology of Sichuan Province (No. 2021YFH0030).

References

Amadei B (1996). Importance of anisotropy when estimating and measuring *in situ* stresses in rock. Int J Rock Mech Min Sci Geomech Abstr, 33(3): 293–325

Du K, Li X, Tao M, Wang S (2020). Experimental study on acoustic emission (AE) characteristics and crack classification during rock fracture in several basic lab tests. Int J Rock Mech Min Sci, 133: 104411

Hakala M, Kuula H, Hudson J A (2007). Estimating the transversely isotropic elastic intact rock properties for *in situ* stress measurement data reduction: a case study of the Olkiluoto mica gneiss, Finland. Int J Rock Mech Min Sci, 44(1): 14–46

Heng S, Guo Y, Yang C, Daemen J J K, Li Z (2015). Experimental and theoretical study of the anisotropic properties of shale. Int J Rock Mech Min Sci, 74: 58–68

Hou P, Gao F, Yang Y G, Zhang X X, Zhang Z Z (2016). Effect of the layer orientation on mechanics and energy evolution characteristics of shales under uniaxial loading. Int J Min Sci Technol, 26(5): 857–862

Hu X, Su G, Chen G, Mei S, Feng X, Mei G, Huang X (2019). Experiment on rockburst process of borehole and its acoustic emission characteristics. Rock Mech Rock Eng, 52(3): 783–802

Jaeger J C (1960). shear failure of anisotropic rock. Geol Mag, 97(1): 65–72

Jarvie D M, Hill R J, Ruble T E, Pollastro R M (2007). Unconventional shale-gas systems: the Mississippian Barnett Shale of north-central Texas as on model for thermogenic shale-gas assessment. AAPG Bull, 91(4): 475–499

JCMS-Ⅲ B5706 (2003). Monitoring method for active cracks in concrete by acoustic emission. Japan: Federation of Construction Materials Industries

Jia Z Q, Xie H P, Zhang R, Li C B, Wang M, Gao M, Zhang Z, Zhang Z (2020). Acoustic emission characteristics and damage evolution of coal at different depths under triaxial compression. Rock Mech Rock Eng, 53(5): 2063–2076

Johnston J E, Christensen N I (1995). Seismic anisotropy of shales. J Geophys Res Solid Earth, 100(B4): 5991–6003

Kim H, Cho J W, Song I, Min K B (2012). Anisotropy of elastic moduli, P-wave velocities, and thermal conductivities of Asan Gneiss, Boryeong Shale, and Yeoncheon Schist in Korea. Eng Geol, 147–148: 68–77

Li X Y, Lei X L, Li Q, Li X C (2017). Experimental investigation of Sinian shale rock under triaxial stress monitored by ultrasonic transmission and acoustic emission. J Nat Gas Sci Eng, 43: 110–123

Nataf G F, Castillo-Villa P O, Baró J, Illa X, Vives E, Planes A, Salje E K H (2014). Avalanches in compressed porous SiO_2-based materials. Physical Review E, 90(2): 022405

Niandou H, Shao J F, Henry J P, Fourmaintraux D (1997). Laboratory investigation of the mechanical behaviour of Tournemire shale. Int J Rock Mech Min Sci, 34(1): 3–16

O'Brien N, Slatt R M (2012). Argillaceous Rock Atlas. New York: Springer Science & Business Media

Ohno K, Ohtsu M (2010). Crack classification in concrete based on acoustic emission. Constr Build Mater, 24(12): 2339–2346

Ohtsu M, Okamoto T, Yuyama S (1998). Moment tensor analysis of Acoustic Emission for cracking mechanisms in concrete. ACI Struct J, 95: 87–95

Rybacki E, Meier T, Dresen G (2016). What controls the mechanical properties of shale rocks? — Part II: brittleness. J Petrol Sci Eng, 144: 39–58

Rybacki E, Reinicke A, Meier T, Makasi M, Dresen G (2015). What controls the mechanical properties of shale rocks? — Part I: strength and Young's modulus. J Petrol Sci Eng, 135: 702–722

Sethna J P, Dahmen K A, Myers C R (2001). Crackling noise. Nature, 410(6825): 242–250

Shannon C E (1948). A mathematical theory of communication. Bell Syst Tech J, 27(3): 379–423

Sheng M, Tian S, Li G, Ge H, Liao H, Li Z (2017). Shale rock fragmentation behaviors and their mechanics by high pressure waterjet impinging. Sci Sin Phy Mech & Astro, 47(11): 114610

Simpson N D J, Stroisz A, Bauer A, Vervoort A, Holt R M (2014). Failure mechanics of anisotropic shale during Brazilian tests. American Rock Mech Assoc, 14–7399

Tian Y, Yu R G, Zhang Y, Zhao X B (2020). Application of acoustic emission characteristics in damage identification and quantitative evaluation of limestone. Adv Eng Sci, 52(3): 115–122 (in Chinese)

Wang J, Xie L Z, Xie H P, Ren L, He B, Li C B, Yang Z P, Gao C (2016). Effect of layer orientation on acoustic emission characteristics of anisotropic shale in Brazilian tests. J Nat Gas Sci Eng, 36: 1120–1129

Worotnicki G (1993). CSIRO triaxial stress measurement cell. In: Hudson J A, ed. Rock Testing and Site Characterization: Principles, Practice and Projects. Oxford: 329–394

Wu S, Ge H K, Wang X Q, Meng F B (2017). Shale failure processes and spatial distribution of fractures obtained by AE monitoring. J Nat Gas Sci Eng, 41: 82–92

Yang S Q, Yin P F, Huang Y H (2019). Experiment and discrete element modelling on strength, deformation and failure behaviour of shale under Brazilian Compression. Rock Mech Rock Eng, 52(11): 4339–4359

Yuan X P, Liu H Y, Wang Z Q (2012). An interacting crack-mechanics based model for elastoplastic damage model of brittle materials under compression. Chinese Solid Mech, 33(6):592–602

Zhu Z Q, Zeng Y W (2005). Study on uniaxial compressive strength and shear failure surface of layered rock mass. Geotech Eng World, 8(4): 27–29